



Pressure-induced first-order antiferromagnetic to ferromagnetic transition in MnN



Xu Zheng ^a, Jiao Tan ^b, Qianqian Wang ^{b,c,*}, Chan Gao ^a, Xiaohui Yu ^b, Wenhui Xie ^c, Yifeng Yang ^{b,**}, Yujie Wang ^a, Changqing Jin ^{b,**}

^a Department of Physics, Chengdu University of Technology, Chengdu 610059, Sichuan, China

^b Beijing National Laboratory for Condensed Matter Physics and Institute of Physics, Chinese Academy of Sciences, Beijing 100190, China

^c School of Physics and Materials Science, Engineering Research Center for Nanophotonics and Advanced Instrument, East China Normal University, Shanghai 200062, China

ARTICLE INFO

Article history:

Received 24 September 2022

Received in revised form 13 November 2022

Accepted 15 November 2022

Available online 17 November 2022

Keywords:

Nitrides

High pressure

Antiferromagnetic

Ferromagnetic

Magnetic transition

Structural transition

ABSTRACT

MnN systems have been widely used to investigate Mn incorporated into III-V compounds, which combines the spin and electron charge as promising diluted magnetic semiconductors (DMS). However, few experiments have demonstrated the magnetic transformation of MnN with lattice constant changes, although it has been mentioned many times in previous theoretical calculations. In this study, we synthesize MnN single crystal under high pressure and temperature. Furthermore, we perform high-pressure resistance, magnetic resistance and synchrotron radiation on MnN single crystal/polycrystalline and observe the first-order phase transition accompanied with antiferromagnetic (AFM) to ferromagnetic (FM) magnetic structure transition under 34 GPa. The experimental result and first-principles calculations reveal the same magnetic and structural transition of MnN in the compression process from equilibrium volume 18.2 to 16 Å³. An analysis of electronic structure and magnetic interactions in terms of the Heisenberg Hamiltonian indicates a strong FM coupling in the [001] plane due to the double exchange mechanism of Mn eg orbitals. With the reduced Mn-N bond length under high pressure, the enhanced FM double exchange interactions could induce the magnetic transition from AFM to FM and subsequently lead to a structural transition from a face-centered tetragonal structure to a cubic structure. These findings provide the foundations for GaMnN or MnN layer DMS.

© 2022 Elsevier B.V. All rights reserved.

1. Introduction

In recent years, the integration of electron charge and spin as promising materials for innovative spin-based devices has attracted the attention of the scientific community. Of particular interest are diluted magnetic semiconductors (DMS), where the transition metal Mn is incorporated into III-V compounds, for example, GaMnN, (MnN)₁/(GaN)₁, (MnN)₁/(AlN)₁, etc [1–6]. However, the synthesis of DMS is extremely difficult owing to the easy formation of metal clusters in these alloys. Furthermore, it is not yet possible to control the magnetism in DMS, i.e., ferromagnetic or antiferromagnetic. Several theories have been proposed to explain the nature of

magnetism in these alloys [7–10]. But the effect of substituting Mn on the cation site on the magnetism is not well established. For this task, several ab initio studies of the MnN system are available that are well related to Mn doped in GaN and other III-V alloys, as Mn atoms in MnN can be found in the same local environment as in diluted alloys [11,12]. Therefore, the study of MnN will provide a better understanding of the nature of Mn coordinated with N in DMS.

Under MnN systems, the crystal structure of MnN at ambient pressure is the tetragonally distorted NaCl-type with antiferromagnetic (AFM) configuration along the [001] direction consists of ferromagnetic (FM) layers, with 3.3 μ_B of Mn lying in the [001] plane [13]. Moreover, the structure and magnetic ordering could be changed with lattice expansions as predicted by first-principles calculations [14,15]. For example, the wurtzite structure with larger equilibrium lattice constants has a ground state of FM, and the zinc blende structure has the ground state of AFM along the [100] direction, respectively. To investigate the relation between the lattice

* Corresponding author at: Beijing National Laboratory for Condensed Matter Physics and Institute of Physics, Chinese Academy of Sciences, Beijing 100190, China.

** Corresponding authors.

E-mail addresses: qianqian_wang@mymail.sutd.edu.sg (Q. Wang), yifeng@iphy.ac.cn (Y. Yang), jin@iphy.ac.cn (C. Jin).

constant and magnetic properties experimentally, a high temperature has been applied on the MnN system. Unfortunately, the magnetic transition (AFM to FM) was not accompanied by the first-order phase transition. This is because N escaped from the sample and the alloys transitioned to Mn_3N_2 in the high temperature range [16]. Suzuki *et al.* measured the high-temperature X-ray diffraction of MnN under a high pressure of 3.0 GPa, to prevent N from escaping from the MnN system [17,18]. Nonetheless, the relationship between the MnN magnetic moment and lattice constant is not well described and explained. Therefore, the study and description of this relationship is crucial to the design and synthesis of DMS.

In this study, we synthesized a MnN single crystal under high temperature and pressure and studied the lattice constant under high pressure to avoid N from escaping from MnN crystals. The experimentally measured lattice constants were well reproduced in our first-principles calculations. Combining both experiment and theory, we conclude that as the pressure increased, a first-order structural phase transition occurred at 34 GPa, accompanied with an AFM to FM transition. Our findings will be important in the synthesis of DMS and in determining whether metal clusters exist in DMS.

2. Materials and methods

We used the 6×600 t high pressure machine and the pyrophyllite as the pressure medium. The method of pressure measurement is accomplished by the change of metal resistance when the metal appears solid to solid phase transition under different pressure. In this paper, we used Bi(I-II) and Ba(II-III) phase transition. The oil pressure corresponding to the pressure points of 2.55 GPa and 5.5 GPa can be obtained through the metal Bi and Ba. Temperature measurement is establishment of the thermocouple and quantification of the press heating power relationship, the thermocouple is in direct contact with our sample.

High-purity $MnCl_2$ (> 99.9%) and Ca_3N_2 (> 99.9%) powders in the molar ratio of $MnCl_2:Ca_3N_2 = 3:1$ were homogeneously mixed and compacted into cylindrical pellets, graphite furnace and pyrophyllite in turn. Putting the assembly into a cubic press. Then put the cylinder into the BN thermal insulation layer, and BN thermal insulation layer in a graphite furnace. To obtain metastable MnN, the reactants were slowly heated to $1000^\circ C$ ($5^\circ C/min$) and 5.5 GPa for 30 min. The run products were washed with distilled HCl to remove the byproduct $CaCl_2$ and unreacted $MnCl_2$, followed by drying in an oven at 348 K.

High-P synchrotron X-ray diffraction experiments were performed using a diamond-anvil cell (DAC) in the Beijing Synchrotron Radiation Facility (BSRF). The obtained polycrystalline MnN was ground into powder and loaded into a sample chamber made of T_{301} stainless-steel gasket with neon as the pressure-transmitting medium. A few ruby balls were loaded into the same sample chamber to serve as the internal pressure standard. The collected angle-dispersive X-ray diffraction data were analyzed by integrating two-dimensional images as a function of 2θ using the program Fit2D to obtain the conventional, one-dimensional diffraction profiles.

The electronic transport properties (RT and MR) of MnN single crystal with high pressure up to 41 GPa were measured using four-probe electrical conductivity methods in a DAC made of CuBe alloy. The diamond culet was $300 \mu m$ in diameter. Au wires with adiameter of $18 \mu m$ were used as electrodes. A T_{301} stainless steel gasket was compressed to $40 \mu m$ with a $150-\mu m$ hole. The cubic BN applied as an insulating layer was pressed into this hole. A small center hole of $100 \mu m$ in diameter was drilled to serve as the sample chamber, where NaCl fine powder served as a pressure-transmitting medium, and a piece of MnN single crystal of dimensions $75 \mu m \times 100 \mu m \times 25 \mu m$ was loaded. The ruby was loaded simultaneously as a pressure marker.

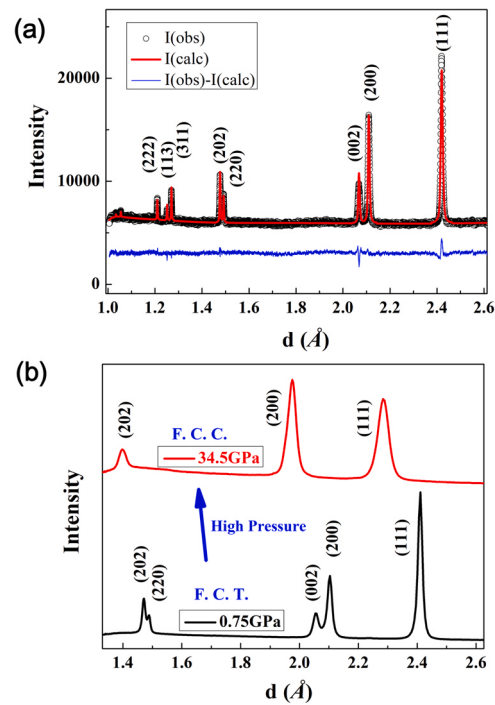


Fig. 1. Rietveld refinement of X-ray diffraction pattern and phase transition under high pressure of MnN. (a) The X-ray diffraction pattern of MnN at room temperature with $\lambda = 1.5405 \text{ \AA}$, black dots are raw observed data in the lab [$I(\text{obs})$], and the red line is the calculated XRD data of MnN [$I(\text{calc})$]. The difference curve [$I(\text{obs}) - I(\text{calc})$] is shown at the bottom in blue. (b) High-pressure synchrotron X-ray diffraction with $\lambda = 0.6199 \text{ \AA}$ of MnN under 0.75 GPa and 34.5 GPa. The face-centered tetragonal (F4/mmm) ambient phase transition to the face-centered cubic (Fm-3m) phase under 34.5 GPa.

Structural relaxation by energy minimization and electronic structure calculations for different magnetic configurations were performed using the full-potential linearized augmented plane-wave method implemented in WIEN2k [19–21]. We used the generalized-gradient approximation with Perdew–Burke–Ernzerhof (GGA-PBE) exchange-correlation energy and 4000 k-point meshes for the Brillouin zone [22,23]. The muffin-tin radii were 2.00 a.u. and 1.60 a.u. for Mn and N, respectively [24]. The maximum modulus for the reciprocal vector K_{max} was chosen such that $R_{MT}^*K_{max} = 7.0$ and $G_{max} = 12$.

3. Results and discussion

The X-ray diffraction data of MnN are shown in Fig. 1(a) and analyzed by the Rietveld method using the General Structure Analysis System software package [25–27]. We identified that the MnN ground state structure belongs to the face-centered tetragonal lattice and F4/mmm space group. The value of the lattice constants ($a=4.221 \text{ \AA}$, $c=4.137 \text{ \AA}$) are larger than those reported by Lihl *et al.* and Otsuka *et al.* Furthermore, the ratio of the lattice constant ($c/a=0.98$) is almost same as those by Lihl *et al.* and Otsuka *et al.*, thus suggesting that the atomic ratio of manganese to nitrogen is almost 1:1 [28,29]. The face-centered tetragonal conventional cell can be transformed into the body-centered tetragonal primitive cell by using a simpler cell selection method (See SM (supplemental material) Fig. S1), so which is not conventional Bravais crystal system. In this paper, in order to more obvious compare the structural transformation between face-centered tetragonal lattice and face-centered cubic, we chose the face-centered tetragonal lattice instead of the body-centered tetragonal lattice. To investigate the relationship between the lattice constant and magnetic properties, high-pressure synchrotron X-ray diffraction was performed on the MnN

polycrystalline in a DAC with neon as the pressure medium and ruby chip for pressure calibration, as shown in SM Fig. S2. As the pressure increases from 0 to 46 GPa, high-pressure synchrotron X-ray diffraction indicates that the pressure-induced structure transition should occur at 34 GPa from the face-centered tetragonal ($F4/mmm$) ambient phase to the face-centered cubic ($Fm-3 m$) phase, which is clearly shown in Fig. 1(b), and the atom coordination of Mn and N are shown in SM Table 1. The compressibility of MnN calculated by the equation of state (EOS) is shown in SM Fig. S3. The MnN is structurally stable up to 34 GPa; when the pressure is larger than 34 GPa, a phase transition to cubic unit cell occurred. A fit to the third-order Birch–Murnaghan EOS of the tetragonal unit cell yields the bulk modulus $B_0 = 198.1$ GPa and $B_0 = 190.4$ GPa for another cubic unit cell. After phase transition, MnN demonstrated poorer compressibility.

Reliable resistivity data are always important to understand the electronic states. Specifically, the magnetic field dependence of resistivity offers an option in electron–electron and electron–spin interactions. As shown in SM Fig. S4, the temperature dependence of resistivity (RT) is measured up to 41 GPa. The resistivity of MnN increases with pressure and always indicates a metal behavior, thus suggesting that the electron structure does not change with the first-order phase transition. The magnetic field dependence of magnetic resistance (MR) at 250 K under various pressures up to 41 GPa is shown in Fig. 2(a). The evolution of the MR shows sharp decreases in 34 GPa, 38 GPa, and 41 GPa, indicating a magnetic transition with the first-order phase transition. According to Marques *et al.*, accompanied with the strain and compression of the lattice parameters, an AFM to FM transition will be observed for the zinc blende polytype and wurtzite structure of MnN [14]. Our experimental data and DFT calculations also present an AFM to FM transition for the NaCl-type structure of MnN with the compressed lattices remaining constant under high pressure. To examine this AFM to FM transition. We measured the temperature-dependence magnetic moment (MT) of

MnN samples, and the AFM to FM transition was observed around $T_c = 32$ K. It is noteworthy that both the low temperature and high pressure compress the lattice constant. Consequently, with the lattice constants decreased, the AFM to FM transition of the MnN samples occurred under 32 K or 34 GPa. Supported by the DFT calculation below, our result is sufficient to approve this magnetic phase transition from AFM to FM of MnN. Suzuki *et al.* reported the relationship between the lattice constant and magnetic properties of MnN using high temperature; however, the magnetic transition was not accompanied with the first-order phase transition, because N escaped from MnN [12–14]. Compared to using a low/high temperature, a high pressure ensures the stability of the N atoms in MnN. It is well known that, transition metal nitride (TMN_x) is difficult to be synthesized with ideal stoichiometric ratio ($x = 1$) and high nitrogen content ($x > 1$). Since 2003, Zeer *et al.* have successfully synthesized Zr and Hf high nitrogen content compounds, $c\text{-Zr}_3\text{N}_4$ and $c\text{-Hf}_3\text{N}_4$ by using diamond anvil under 15.6–18 GPa, 2500–3000 K. This shows N-atoms should not escape in DAC techniques as compared to the traditional effect of heating, we have measured MnN again after decompressing from high pressure (see SM Fig. S5). It can be seen that the synchrotron radiation diffraction of MnN after pressure decompress from high pressure to 0.1 GPa is in good overlap with the synchrotron radiation of unpressurized MnN in intensity and diffraction peak, which indicates that the N atom does not escape under high pressure, and also indicates that the phase transition of MnN under high pressure is reversible. Moreover, high pressure technique provides not only the pressure dependence MR, RT, and X-ray diffraction, but also the structural-related origin of the transport properties under various pressures. All of these data are important to understand the structure and magnetics transition.

We now discuss the relationship between the lattice constants and magnetic transition. As shown in Fig. 2(c), in the magnetic structure according to Suzuki *et al.*, each Mn-ion has twelve nearest-neighboring Mn-ions coupled by superexchange interactions

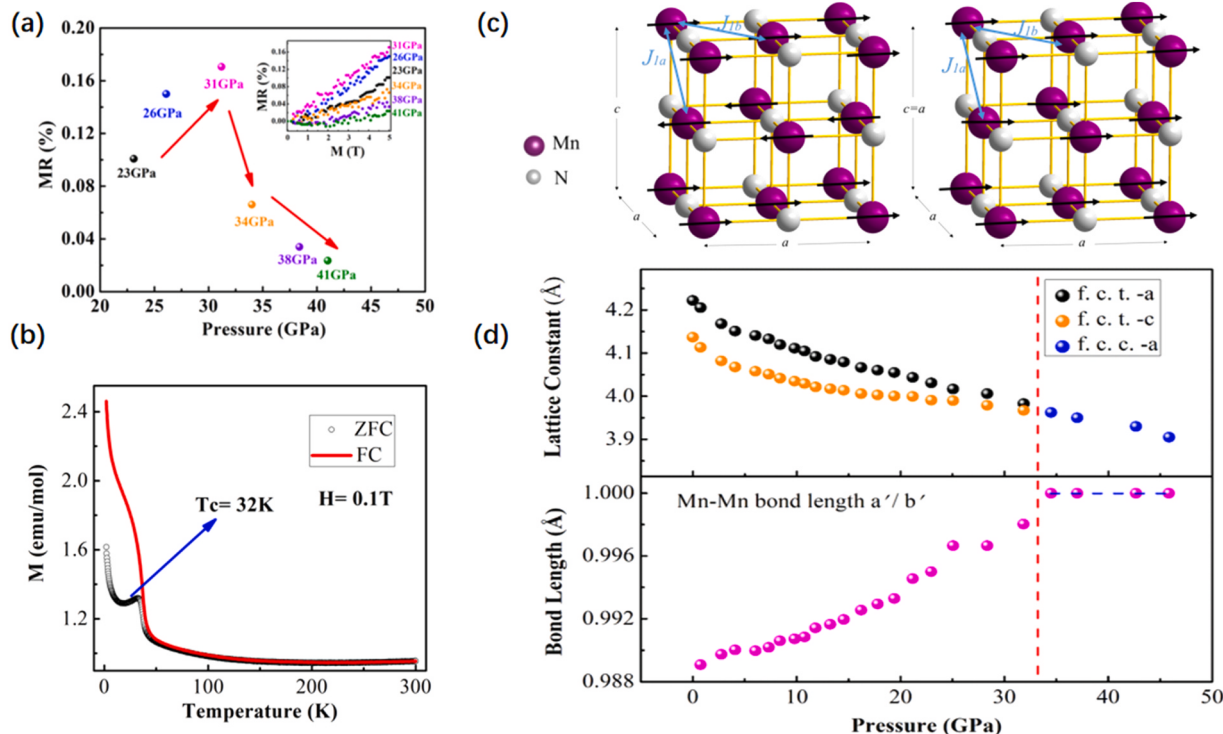


Fig. 2. (a) Temperature dependence of MR at 250 K (5Tesla) under various pressures up to 41 GPa; Inset figure is temperature dependence of MR at 250 K (0–5Tesla) under various pressures up to 41 GPa. The circle represents the original magnetoresistance data at different pressures. (b) Temperature dependence of DC magnetization of MnN with $H = 0.1$ T. (c) Antiferromagnetic and ferromagnetic structure of MnN with face-centered tetragonal lattice. (d) The ratio of a' and b' (Mn–Mn bond length) as well as the lattice constants a and c .

through the intermediate N-ions with a Mn–N–Mn bond angle of 90°. Four of these Mn-ions are on the same *ab* plane, and couple ferromagnetically with the central Mn-ion. Eight are on adjacent planes, and couple antiferromagnetically with the central Mn-ion. Furthermore, there are six next-nearest-neighboring Mn-ions coupled ferromagnetically with the central Mn-ion by a 180° superexchange interaction via the N-ions [17,18]. For simplicity, we consider here only the nearest-neighbor Mn-ions and define J_{1a} as the exchange interaction of the central Mn-ion with the eight Mn-ions in the adjacent planes and J_{1b} as that with the four Mn-ions in the same *ab* plane and denote the corresponding bond lengths as a' and b' , respectively. With increasing pressure, the lattice constants a and c decrease and the Mn–Mn bond lengths vary accordingly. We found that for pressures below 34 GPa, $a'/b' < 1$, and the coexisting ferromagnetic J_{1b} and antiferromagnetic J_{1a} yields an AFM magnetic structure of MnN as observed at ambient pressure. While for pressures above 34 GPa, we obtain a cubic structure with the Mn–Mn bond length $a'/b' = 1$. The ferromagnetic exchange coupling $J_{1a}=J_{1b}$ yields a FM phase in this high pressure regime. The transition from antiferromagnetic to ferromagnetic J_{1a} should be related to the competition of the superexchange coupling between Mn t_{2g} spins and the double exchange mechanism due to the presence of conducting e_g electrons. The latter becomes dominant at pressures. Therefore, MnN exhibits an AFM-to-FM transition accompanied by a first-order structural transition. These relationships are well examined by first-principle calculations in the following.

The structural and magnetic transitions of MnN under high pressure were investigated by first-principles calculations using the generalized-gradient approximation with the Perdew–Burke–Ernzerhof (GGA-PBE) exchange-correlation potential for different magnetic configurations. The settings of FM, AFM1 and AFM2 configurations are shown in Fig. 3(a). At ambient pressure, the AFM ordering along the

[001] direction (AFM1) was found to be the ground state for the face-centered tetragonal MnN. The GGA-PBE calculated equilibrium volume V_0 of 18.2 Å³ is larger than those of previous works but $c/a = 0.98$ is in good agreement with the previous theoretical calculations and neutron diffraction experiment [30]. As shown in Fig. 3(b), the calculated lattice constants with varying pressure were in excellent agreement with the experimental measurements and confirmed a transition from the face-centered tetragonal to cubic structure at high pressures. Correspondingly, as shown in Fig. 3(c), the total energy of the FM state decreases faster than that of the AFM1 state with increasing pressure and an AFM–FM magnetic transition was found as the volume is compressed to 16 Å³, which corresponds to a pressure of 34 GPa, consistent with the experimental MR data. PBE calculations of MnN with experimental lattice constants were also performed for different magnetic states. As shown in Fig. S6, the magnetic transition from AFM to FM occurred at 34 GPa, in good agreement with the experimental data. As a conclusion, the first-principle calculations indicate that the structural transition should be accompanied with the AFM-to-FM transition. We should note that at the magnetic transition, the optimized a/c ratio with AFM1 phase still shows a tetragonal lattice, but the given lattice constants are very close to the cubic phase. Thus, it is expected that the transition should be a weak first-order structural transition induced by the AFM–FM transition.

To discuss the relationship between the lattice constants and the magnetic transition, the magnetic exchange interactions were calculated using the classical Heisenberg model:

$$H = -\sum_{<ij>} J_{ij} S_i \cdot S_j$$

The J values in MnN with compressed volume are shown in Fig. 3(d). For MnN with face-centered tetragonal structure, the magnetic interactions between Mn atoms can be discussed with J_{1a} and J_{1b} [11,31–33]. At ambient pressure, the J_{1a} between Mn-ions in adjacent planes is dominated by the AFM superexchange coupling ($J_{1a} = -9.6$ meV) due to half-filled t_{2g} orbitals [34], while the

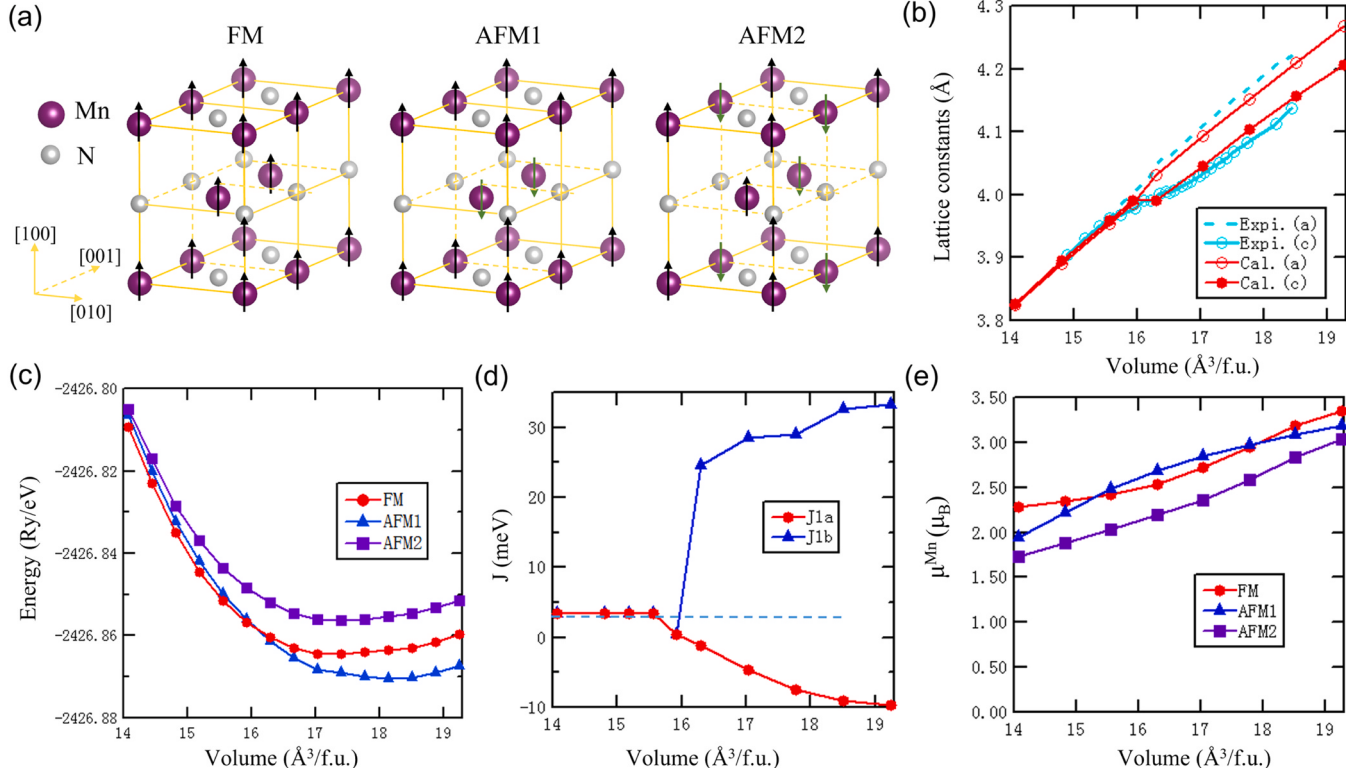


Fig. 3. (a) The FM, AFM1 and AFM2 configurations. The superlattice of body-centered tetragonal primitive cell are plotted for clearly illustration of the magnetic configurations. (b) Total energy vs. volume of MnN for FM, AFM1, and AFM2 states. (c) The optimized lattice constants considering FM, AFM1, and AFM2 states vs. volume and the comparison with experimental data. (d) The exchange parameter J_{1a} and J_{1b} calculated from the Heisenberg model with the optimized lattice constants vs. volume. (e) The magnetic moments of Mn atom for FM, AFM1, and AFM2 states with the optimized lattice constants vs. volume.

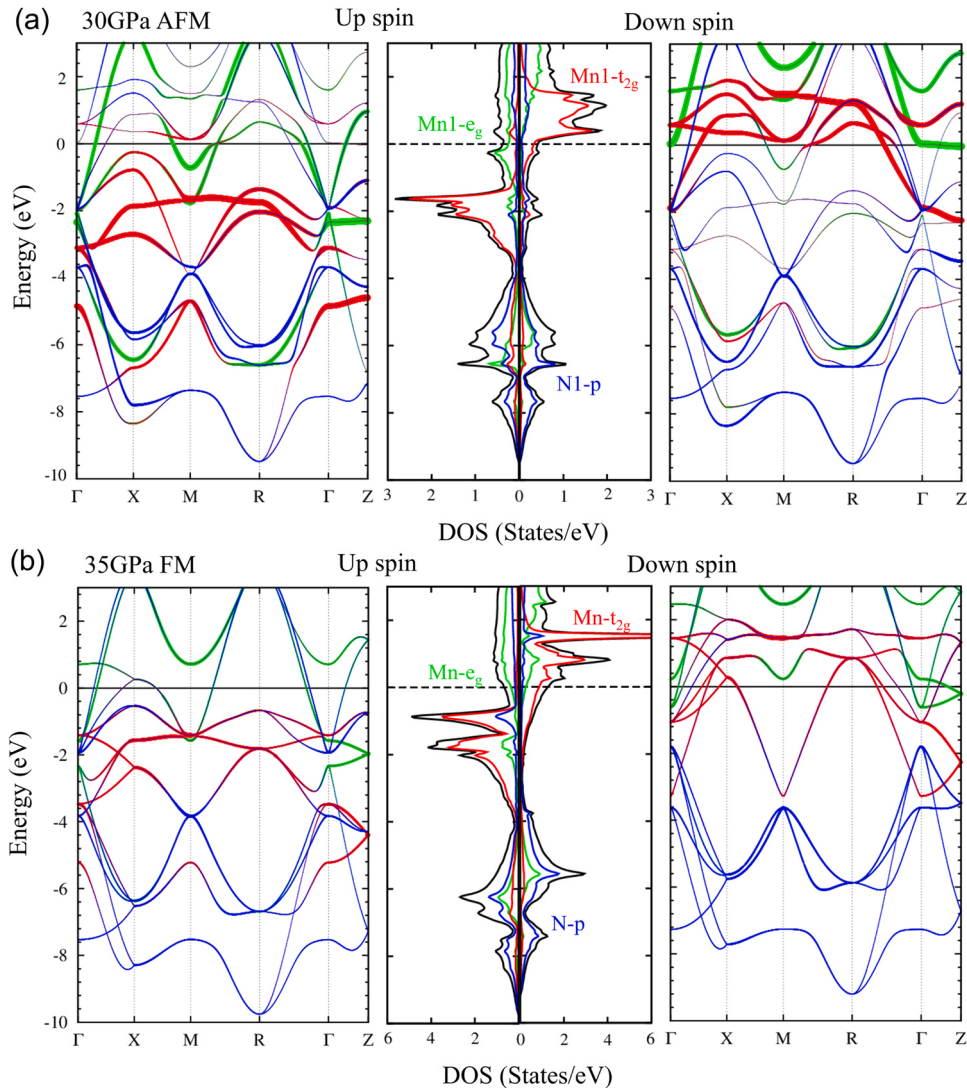


Fig. 4. (a) Partial density of states (PDOS) of the AFM state under 31.8 GPa with the experimental lattice constants (b) Partial density of states (PDOS) of the FM state under 34.5 GPa with the experimental lattice constants.

ferromagnetic J_{1b} originates from the 90° Mn–N–Mn double-exchange interactions inside the ab plane involving the Mn e_g state and N-p orbitals (dpσ hybridization) ($J_{1b} = 33$ meV) [35]. The FM double exchange interactions are larger than the AFM interactions, implying a strong hybridization between the Mn- e_g orbitals and the N-p orbitals. For the cubic structure above 34 GPa, the lattice constants change to $c/a=1$ with equal Mn–N bond length along the [001] direction and in the same [001] plane. For the 12 nearest-neighbor Mn–Mn coupling, competition exists between superexchange (AFM) and double-exchange (FM) interaction, resulting in a slight FM coupling ($J_{1a} = J_{1b} = 3.5$ meV), as shown in Fig. 3(d). In fact, the Anderson–Hasegawa model [36] predicts the FM double exchange rather than AFM superexchange when only one e_g electron exists per Mn atom. Therefore, the ground state of the rock-salt structure is FM. We should note that the fact $J_{1b} = 0$ at the transition could be artificial due to our much simplified model. In reality, one should also consider the next-nearest-neighbor Mn-ions and the exact value of J_{1b} will be corrected. However, the qualitative variation of both J_{1a} and J_{1b} with pressure is verified by the special AFM and FM configurations below and above 34 GPa.

To rationalize the structure transition from the face-centered tetragonal structure to cubic rock-salt structure under high pressure, we can illustrate it in two steps: first, the competition between

magnetic interactions results in the ground state magnetic ordering with the compressed volume; next, the structure is stabilized in terms of minimized energy with the ground magnetic configuration. Thus, with the magnetic transition from AFM to FM under high pressure, a shear strain from the magnetic force is applied onto the (001) plane that induces the structural transition, in accordance with the experimental finding.

Fig. 3(e) presents the magnetic moments of MnN under high pressure for different magnetic configurations. As was shown, the magnetic moments decrease with pressure, owing to the enhanced Mn-d and N-p coupling resulted from the decreased Mn–N bond length. The magnetic moments were found to decrease from $3.18 \mu_B$ to $1.94 \mu_B$ of the AFM1 state, and decrease from $3.34 \mu_B$ to $2.27 \mu_B$ for the FM state with the compressed volume from 19.3 \AA^3 to 14 \AA^3 , thus supporting an enhanced double exchange mechanism at high pressures.

The electronic structures of MnN under high pressure were further investigated. Fig. 4 shows both band structure and partial density of states (PDOS) of the AFM state under 31 GPa and FM state of MnN under 35 GPa in terms of the Mn d e_g , Mn d t_{2g} , and N p states, respectively. Both of the band structure of AFM and FM states reveal the metal nature of MnN under high pressure. For the DOS of AFM state, the spin-up DOS on one Mn equals the spin-down DOS on

the other Mn. Thus, only one of two Mn atoms is shown. As shown in Fig. 4(a), the majority filled t_{2g} bands lie entirely below the Fermi level from -4–0 eV with three electrons while the minority spin t_{2g} bands are pushed above the Fermi level from 0 eV to 2 eV. The majority e_g is filled with only one electron from -1–0 eV, while the minority e_g is above the Fermi level. Moreover, the e_g bands have both spin up and spin-down contributions to the bonding states with N-p orbitals below the Fermi level from -7 eV to -4 eV. For the PDOS of the FM state, the spin-up DOS is the same as the spin-down DOS; thus, the DOS of two Mn atoms are as shown in Fig. 4(b). The DOS of the FM state is similar to that of the AFM state. These results suggest that MnN remains a metallic state in the whole pressure range and support our discussions concerning the origin of the exchange interactions among nearest-neighboring Mn-ions.

4. Conclusion

In summary, we combined DAC techniques and first-principle calculations to study the relationship between phase and AFM-to-FM transition with the change in the MnN lattice constant. We observed experimentally that it is necessary to apply a high pressure up to 34 GPa, and as the lattice constant decreased the first-order phase transition and AFM-to-FM transition occurred. The first-principles calculations indicated that the structural transition of MnN under high pressure from the face-centered tetragonal structure to the cubic structure was driven by magnetic forces owing to the magnetic transition from AFM1 to FM. The strong FM double-exchange interactions arising from the Mn d e_g state and N-p state were crucial in determining the magnetic structures in MnN. Our results suggested that both the Mn doping to the III-V compounds and the MnN layers in DMS will present the FM state, if these inclusions were strained; if the system was exposed to an extremely strong hydrostatic strain, the system will present an FM state. Furthermore, if DMS were present in the FM ground state in the range of the AFM lattice constant, it is highly likely that the Mn atom clusters exist in these alloys. Finally, these findings provided the groundwork for future studies of DMS of III-V compounds and highlighted the potential opportunities for the design of electron charges and spin materials.

CRediT authorship contribution statement

Xiaohui Yu, Yifeng Yang and Changqing Jin conceived the project and designed experiments. Xu Zheng and Jiao Tan carried out the experiments. Qianqian Wang calculated the structure and magnetic transition. Xu Zheng, Qianqian Wang, Chan Gao, Xiaohui Yu, Wenhui Xie, Yifeng Yang, Yujie Wang and Changqing Jin wrote the paper. All authors contributed to interpretation and presentation of the results.

Data availability

No data was used for the research described in the article.

Declaration of Competing Interest

The authors declare that they have no known competing financial interests or personal relationships that could have appeared to influence the work reported in this paper.

Acknowledgments

This study were partially supported by Synergic Extreme Condition User Facility (SECUF). We are grateful for the high-pressure synchrotron X-ray experiments performed at the high-pressure station of the BSRF. This work supported by Natural Science

Foundation of Sichuan Province (No. 2022NSFSC0332 and No.2023NSFSC4704), and China Postdoctoral Science Foundation (2019TQ0039).

Appendix A. Supporting information

Supplementary data associated with this article can be found in the online version at doi:[10.1016/j.jallcom.2022.168120](https://doi.org/10.1016/j.jallcom.2022.168120).

References

- [1] M. Zaja, C. R. Doradzinski, J. Gosk, J. Szczytko, M. Lefeld-Sosnowska, M. Kaminska, A. Twardowski, Magnetic and optical properties of GaMnN magnetic semiconductor, *Appl. Phys. Lett.* 78 (2001) 1276.
- [2] H. Heddar, A. Zaoui, M. Ferhat, Magnetic behavior of (MnN)1/(AlN)1, (MnN)1/(GaN)1, and (MnN)1/(InN)1 superlattices, *Superlattice. Microstruct.* 53 (2013) 16.
- [3] J. Guerrero-Sánchez, N. Takeuchi, Antiferromagnetic MnN layer on the MnGa (001) surface, *Appl. Surf. Sci.* 390 (2016) 328.
- [4] M. Zajaac, J. Gosk, M. Kaminska, A. Twardowski, T. Szyszko, S. Podsiadlo, Paramagnetism and antiferromagnetic d-d coupling in GaMnN magnetic semiconductor, *Appl. Phys. Lett.* 79 (2001) 2432.
- [5] M. Kaminski, S. Podsiadlo, P. Dominik, K. Woźniak, L. Sobczykki, R. Jakielka, A. Barcz, M. Psoda, J. Mizera, R. Bacewicz, M. Psoda, J. Mizera, R. Bacewicz, M. Zajac, A. Twardowski, New chemical method of obtaining thick Ga(1-x)Mn(x) N layers: prospective spintronic material, *Chem. Mater.* 19 (2007) 3139.
- [6] S. Podsiadlo, T. Szyszko, W. Gebicki, J. Gosk, R. Bacewicz, L. Dobrzański, K. Woźniak, M. Zajac, A. Twardowski, Synthesis of bulk Ga_{1-x}Mn_xN: a prospective spintronic material, *Chem. Mater.* 15 (2003) 4533.
- [7] M. Marques, L.M.R. Scolfaro, L.K. Teles, J. Furthmüller, F. Bechstedt, L.G. Ferreira, Theoretical prediction of ferromagnetic MnN layers embedded in wurtzite GaN, *Appl. Phys. Lett.* 88 (2006) 022507.
- [8] J.A. Chan, Jefferson Z. Liu, Hannes Raebiger, Stephan Lany, Alex Zunger, Relative stability, electronic structure, and magnetism of MnN and (Ga,Mn)N alloys, *Phys. Rev. B* 78 (2008) 184109.
- [9] J.M.D. Coey, M. Venkatesan, C.B. Fitzgerald, Donor impurity band exchange in dilute ferromagnetic oxides, *Nat. Mater.* 4 (2005) 173.
- [10] A. Alsaad, M. Bani-Yassein, I.A. Qattan, A. Ahmad, S.R. Malkawi, Structural and magnetic properties of MnN and ScN binaries and their ScN:Mn diluted magnetic semiconductors and Mn_xSc_{1-x}N alloys, *Phys. B* 405 (2010) 1408.
- [11] A. Janotti, S.H. Wei, L. Bellaiche, Electronic and magnetic properties of MnN versus MnAs, *Appl. Phys. Lett.* 82 (2003) 766.
- [12] R. de Paiva, J.L.A. Alves, R.A. Nogueira, J.R. Leite, L.M.R. Scolfaro, First-principles materials study for spintronics: MnAs and MnN, *Braz. J. Phys.* 34 (2004) 568.
- [13] K. Suzuki, Y. Yamaguchi, T. Kaneko, H. Yoshida, Y. Obi, H. Fujimori, H. Morita, Neutron diffraction studies of the compounds MnN and FeN, *J. Phys. Soc. Jpn.* 70 (2001) 1084.
- [14] M. Marques, L.K. Teles, L.M.R. Scolfaro, J. Furthmüller, F. Bechstedt, L.G. Ferreira, Magnetic properties of MnN: Influence of strain and crystal structure, *Appl. Phys. Lett.* 86 (2005).
- [15] M.S. Miao, W.R.L. Lambrecht, Structure and magnetic properties of MnN, CrN, and VN under volume expansion, *Phys. Rev. B* 71 (2005) 214405.
- [16] M. Tabuchi, M. Takahashi, F. Kanamaru, Relation between the magnetic transition-temperature and magnetic-moment for manganese nitrides MnN, *J. Alloy. Compd.* 210 (1994) 143.
- [17] K. Suzuki, T. Kaneko, H. Yoshida, Y. Obi, H. Fujimori, H. Morita, Crystal structure and magnetic properties of the compound MnN, *J. Alloy. Compd.* 306 (2000) 66.
- [18] K. Suzuki, T. Suzuki, Y. Fujinaga, T. Kaneko, H. Yoshida, Y. Obi, S. Tomiyoshi, Anomalous thermal expansion of MnN, *J. Alloy. Compd.* 360 (2003) 34.
- [19] P. Blaha, K. Schwarz, G. Madsen, D. Kvásnicka, J. Luitz, Wien2k: an augmented plane wave local orbitals program for calculating crystal properties, *J. Endocrinol.* (2010).
- [20] O.K. Andersen, Linear methods in band theory, *Electronic Structure of Complex Systems*, Proc. a NATO Adv. Study Inst. 11 (1984).
- [21] G. Kresse, J. Furthmüller, Efficient iterative schemes for ab initio total-energy calculations using a plane-wave basis set, *Phys. Rev. B* 54 (1996) 11169.
- [22] J.P. Perdew, K. Burke, M. Ernzerhof, Generalized gradient approximation made simple, *Phys. Rev. Lett.* 78 (1997) 1396.
- [23] H.J. Monkhorst, J.D. Pack, Special points for brillouin-zone integrations, *Phys. Rev. B* 13 (1976) 5188.
- [24] O.K. Andersen, T. Saha-Dasgupta, Muffin-tin orbitals of arbitrary order, *Phys. Rev. B* 62 (2000) R16219.
- [25] H.M. Rietveld, A profile refinement method for nuclear and magnetic structures, *J. Appl. Cryst.* 2 (1969) 65.
- [26] B.H. Toby, EXPGUI, a graphical user interface for GSAS, *J. Appl. Cryst.* 34 (2001) 210.
- [27] A.C. Larson, L.E. Gentry, M.B. David, R.A. Cooke, D.A. Kovacic, The role of seepage in constructed wetlands receiving agricultural tile drainage, *Ecol. Eng.* 15 (2000) 91.
- [28] F. Lihl, P. Ettmayer, A. Kutzelnigg, Beitrag zum system mangan-stickstoff, *Z. Met.* 53 (1962) 715.
- [29] N. Otsuka, Y. Hanawa, S. Nagakura, Crystal structure and phase transition of Mn₆N₅ studied by electron diffraction, *Phys. Status Solidi A* 43 (1977) K127.

- [30] R. Rajeswarapalanichamy, A. Amudhavalli, M. Manikandan, M. Kavitha, K. Iyakutti, First principles study of structural and magnetic properties of transition metal nitrides TMN (TM = Cr, Mn), *PhaseTransit* 90 (2017) 894.
- [31] W.R.L. Lambrecht, M. Prikhodko, M.S. Miao, Electronic structure and magnetic interactions in MnN and Mn₃N₂, *Phys. Rev. B* 68 (2003) 174411.
- [32] M. Wierzbowska, D. Sanchez-Portal, S. Sanvito, Different origins of the ferromagnetic order in (Ga,Mn)As and (Ga,Mn)N, *Phys. Rev. B* 70 (2004) 235209.
- [33] W.R.L. Lambrecht, M.S. Miao, P. Lukashev, Magnetic properties of transition-metal nitrides, *J. Appl. Phys.* 97 (2005) 11.
- [34] A. Filippetti, N.A. Hill, Magnetic stress as a driving force of structural distortions: The case of CrN, *Phys. Rev. Lett.* 85 (2000) 5166.
- [35] D.I. Khomskii, G.A. Sawatzky, Interplay between spin, charge and orbital degrees of freedom in magnetic oxides, *Solid State Commun.* 102 (1997) 87.
- [36] P.W. Anderson, H. Hasegawa, Considerations on double exchange, *Phys. Rev.* 100 (1955) 675.